Star Formation Rates in Interacting Galaxies

Emma Bacarra,[1]

In Collaboration With

Maggie Vickers,[1] Madison Ringham,[1]

[1]*University of Washington*
Department of Astronomy

ABSTRACT

Stellar formation rates are an important aspect in characterizing the Universe at a large scale. To study these characteristics, this project proposes the use of H-α Balmer Lines to compare rates between interacting galaxies and non-interacting galaxies. Collecting images from a Charge-Coupled Device, the raw image data was adjusted with calibration frames and analyzed over histograms and pixel values. It was observed that the chosen interacting galaxies, NGC 4567 & NGC 4568, had comparable stellar formation rates to the chosen non-interacting galaxy, M 58. However, it is noted that further study with additional objects should be done in order to generalize the characteristics of interacting galaxies and their impact on stellar formation rates.

1. INTRODUCTION

Stellar formation rates, or SFRs, are some of the ways used to characterize the Universe. They can reveal dynamic histories and evolution of the galaxies seen today. At high redshifts, or the shift of light towards longer or redder wavelengths, it has been observed that objects have greater stellar formation activity. Along with long, static periods, formation rates can come and go in the form of spontaneous bursts, making it a hard number to precisely quantify (Boquien et al. (2014)). To understand the characteristics of galactic evolution is to work towards characterizing the Universe in a large scale context.

A robust way of studying the star formation rates of objects requires the measurement of their Balmer lines. More specifically, the H-α Balmer line, which describes specific photon emissions of hydrogen atoms. This is one of the most popular methods, taking advantage of emission lines as a product of the recombination of hydrogen (Tacchella et al. (2022)). During star formation, hydrogen gas is ionized in the process due to the collision of dense molecular gas clouds. As a result, these hydrogen ions emit photons that can be measured with the help of H-α lines. This method is advantageous as it is a more direct measure of the instantaneous star formation rate and is less susceptible to effects such as dust extinction (Glazebrook et al. (1999)).

Known as the Butterfly Galaxies, or Siamese Twins, NGC 4567 and NGC 4568 are a pair of interacting galaxies located in the Virgo Cluster. At a distance of 59 million light years away, these two galaxies are merging together and have already made contact in their outer regions. Because of their closeness, the gasses between the two galaxies have begun to interact, thus activating a new region of stellar formation activity. The upper, blueish galaxy is NGC 4567 and the lower, orange galaxy is NGC 4568. This pair of galaxies was discovered by William Herschel during a series of observations in 1784 (Herschel (1786)).

M 58, a non-interacting galaxy, is another member of the Virgo Cluster within a radius of 15 degrees from the Butterfly Galaxies. It is nicknamed the Ring Bearer Galaxy and is one of the earliest known spiral galaxies. Among the brightest in its cluster, M 58 was argued to be farthest known astronomical object after its discovery in 1779 by Charles Messier (Hartmut Frommert (1996)). In the same year of the discovery of NGC 4567 and NGC 4568, M 58 was also recorded in William Herschel's observations.

This research project analyzed the effects of interacting galaxies on their star formation rates. The objects chosen for observation were NGC 4567 & NGC 4568 and M 58 to observe their brightness with an R-band filter (radio wavelength), G-band filter, I-band filter, and H-α filter. Then, the average brightness was subtracted from the total to isolate the H-α lines. As discussed, it is safe to assume that the H-α lines are purely caused by the presence of hydrogen ionization, pointing to stellar formation activity in O-type stars.

Once isolated, the intensities of the brightness at H-α with other objects is studied and compared - namely, the H-α lines of nearby interacting galaxies were investigated to analyze the impacts on their SFRs by comparing them with standalone galaxies to estimate stellar formation rates.

With the image data collected from the ARCSAT Telescope from Apache Point Observatory (APO), these initial questions were kept in mind: 1) How long does it take to get a proper measurement of H-α lines? and 2) What are some back-up plans in terms of finding other ways to estimate SFRs in the event that H-α lines can't be measured (due to weather, etc)? To hypothesize, it was anticipated that the stellar formation rates of NGC 4567 and NGC 4568 would be observed to be less than the stellar formation rate of galaxy M 58.

2. METHODOLOGY

2.1. *Star Formation Rate Derivation*

Under the guidance of Professor Tuttle, and various sources of external research groups, the star formation rates of the target objects were characterized by attempting to subtract the red-shifted H-α Balmer line from the R-band filter (Glazebrook et al. (1999)). What makes them optimal for quantifying stellar formation rates is their sensitivity to even the faintest of activity and the ability to trace recent formations in high mass stars (James et al. (2004)). However, the high sensitivity of H-α emissions comes at the risk of being susceptible to noisy data. Obtaining H-α emissions from an object requires extensive exposure times, allowing the interference of noise and pollution to build up. As a method of de-noising, calibration frames (darks, biases, and flats) were used to remove data contamination from the raw images. Measurements were also increased to higher precision by stacking several images to create a master frame with the median combination method.

2.1.1. *Darks*

Darks are the calibration frames that reduce hot pixel noise and amp glow, or the glare created from the camera. They are advantageous in improving the proportions between signal and noise in an image. The noise can originate from various places depending on exposure, temperature, and ISO. Darks are especially important in CMOS cameras, which is the other type of electronic detector along with Charge-Coupled Devices (CCDs). This project obtained the photometric data from a CCD.

Because noise can depend on various exposures and temperatures, darks are situationally-based and should match the conditions of the raw images. That way, a record of a pure noise frame can be subtracted to remove unwanted pollution. To improve the subtraction values, it is typical for 20-30 frames to be taken, although greater numbers can further improve noise reduction. Hence the name, darks are images captured in darkness with the lens cap on. A collection of darks must be taken for each of the various conditions planned to shoot real images, along with identical settings. Once obtained, the frames must be combined, either with the use of a software or manual programming.

2.1.2. *Biases*

Similar to darks, biases are taken without light exposure. These calibration frames measure the electronic noise generated during the camera's process of reading data obtained from the detector. Known as readout signals, this type of noise is captured by taking extremely short exposures with the lens cap on in darkness. Here, noise from sources such as temperature are not as influential. Multiple frames are optimal for reducing as much noise as possible, and all can be combined into a single master bias frame.

2.1.3. *Flats*

Considered one of the most important for noise reduction, flats is the third kind of calibration framed used in this project. These are images that capture a uniformly illuminated field to account for variations between pixels. Small interferences, like dust, dirt, smudges, or other blemishes, may be difficult to remove with the other two types of calibration frames. They can cause a vignette effect, which appears as an uneven gradient of light around the edges. With flats, capturing an evenly illuminated light source helps to identify those imperfections so they can be removed from the images.

Flats must be taken within close range of the actual images, either during the same observation session or the morning after. Unlike darks and biases, several flats need to be taken for each individual filter in monochrome. The conditions must also match the focus and orientation of the actual images being taken. Once flats for each filter is obtained, each frame must be normalized before stacking each filter together to create master frames. These frames

can also be combined with a software or manual programming. If normalization is applied afterwards, the raw images will not calibrate correctly and continue to appear noisy.

2.2. *Developments for Automation*

As a method of streamlining the plan towards meeting the set goals, the utility of custom classes and functions accelerated the process. A quicker, easier way to go directly from the raw data to flux calculations allowed for a stronger focus on the overall motivations behind the project. The most impactful aspects of these custom developments minimized the required lines of code for both pre-processing and photometric analysis. Built on a dynamic architecture, these classes follow a forward structure and allow for more flexibility in their mechanisms. Although it's customizability can be much stronger, it has been specified well enough to fit the various needs of the user. As an additional advantage, the use of custom functions imported from a secondary Python file allows for minimal confusion from unmatched names of imported packages within the current space.

2.2.1. *Optimizing Image Stacking*

A custom class was built to ease the image stacking process. Within this class contained two relevant custom functions, one for combining the data, and another for stacking generic arrays. The custom stacking function takes the file path to a folder directory containing the fits files intended to be stacked. As the function iterates through each file in the specified folder directory, it extracts the data and does a series of preparations before taking the final list of data and combining into a single array.

The custom stacking function involves these parameters: folder path, new file name, overwrite permission, a keyword for file search query, warning suppressor, and the option to normalize the data before stacking. These parameters are then used in the following steps:

1. Iterate through the located files in the specified directory.

2. When applicable, filter out file names that do not match the optional search query.

3. During an iteration, the file data and the world coordinates are extracted.

4. The pixel coordinates of the image are converted to the World Coordinate System (WCS), using the information extracted from the FITS header.

5. In a list outside of the iterating loop, the image data is appended as a single element and stored for later.

6. Once all of the files' image data becomes an element of the final list, Once the list receives all of the files' image data as its elements, it is then converted to an array to allow for compatibility with numerical manipulation.

7. Passed into the Combiner class from the CCDProc package, the image data is combined with the median combine method.

8. If indicated, the combined data will be written to a new fits file specified by the new path. As a default, the function returns the array to allow for direct use.

During a single iteration, the data's coordinate system was translated from pixels to the World Coordinate System (WCS) using the CCDProc package. This was to account for the shift of the object between images so that it was an easier process to combine them. If the user specifies, this data is then normalized with the other custom function before appending it to the overall list. Once all files have been iterated through, list of image data is then passed into the Combiner class from the CCDProc package, where a median combine method was applied directly afterwards. Then NaN values are filtered out and replaced with 0s, and the custom function either returns it as an array or writes it to a specified file (as determined by the user).

2.2.2. *Rapid Annulus Photometry*

The second most impactful custom program was developed to accelerate the process of aperture photometry. As a separate class from the image stacker, it provides a more autonomous process to perform photometry. The design of the architecture was based on the generalization of a standard performance of photometry. Intended for use after stacking and background subtraction, a simple pass of the intended data activates the class and initializes a collection

of several internal variables. These variables are initialized as None values, and adjusted during the use of the custom functions. Among them, the mechanics of dictionary objects were used to simplify selections for interval and stretch functions during image normalization. There are multiple custom functions built within this photometry class to automate the process.

The Normalizer function is designed to minimize the lines needed for the normalization of image data before plotting. During a standard procedure, a user might have to make several counts of the normalization factor. With Normalizer, that can minimize that part of the process up to a single line. Due to the default settings, this function can be called with up to no parameters, since it accesses the image data's corresponding internal variable. The scaling interval is defaulted to Z-Scale, with a square-root stretch and percentile cropping between 1% and 99.75%. If necessary, these can be adjusted to the user's liking. The photometry class then makes a record of the minimum and maximum values set by the top and bottom percentages. To normalize the data, this function uses the ImageNormalize function from Astropy.Visualization and sets the parameters to corresponding parameters of the Normalizer function and internal variables.

The Sources function contains the procedure for selecting an image segment, finding stellar sources with the DAOStarFinder function of the PhotUtils.Detection package, and generating a table of the captured apertures. Calling Sources requires three parameters: the X and Y dimensions of the image segment, and sigma. As a parameter of the sigma_clipped_stats function from Astropy.Stats, sigma represents the number of standard deviations to use for both the lower and upper clipping limit (Astropy Collaboration et al. (2022)). Optional parameters include: full-width half-maximum (FWHM) and threshold settings for the star finder and the radii of the inner and outer rings of the annulus. The Sources execution process is as described:

1. Based on the X and Y dimensions specified, an image segment is created from the class-internal record of the total image data.

2. The snippet is then recorded into the class-internal variable, which was initialized as a None type object.

3. The mean, median, and standard deviations are calculated using the sigma clipping function from Astropy and recorded in their corresponding internal variables. Clipping removes extreme outliers from the snippet to allow for cleaner calculations.

4. With the DAOStarFinder detection algorithm of PhotUtils, stellar sources are then located within the snippet.

5. The table of located sources is recorded internally and formatted for consistent outputs.

6. Using the set radii and the positions of the sources, the circular regions are defined around them for later calculations.

7. Aperture photometry is performed with the PhotUtils.Aperture package on the original image data using the defined annuli.

8. As an option for external use, the snippet image data and the source table is returned to conclude the function.

Immediately following Sources, the View function was designed to provide a visualization of the image segmentation, located sources, and their apertures. Not only is it practical for visual understanding, but it also allows a user to make external revisions. When a source table is returned from the Sources function, this allows the user to manually remove unwanted sources from the table. With the requirement of a source table as a parameter, the View function then compensates for user edits by updating the source table internally. Consequently, the source positions and their annuli are adjusted accordingly. Once all variables are updated, the View function provides the image data annotated with the segment border and a location of the sources and their annuli:

1. Internal variables are updated based on the source table passed as a required parameter.

2. Utilizes the Normalizer function to generate the normalization factor for image plotting.

3. If preferred, the plot aesthetics are set to a dark mode for better viewing.

4. Using the internal records of the snippet dimensions, the snippet border is generated with the use of Mat-PlotLib.Patches' Rectangle function.

5. Over the plot of the original image data, the snippet border is annotated onto the image.

6. In a second subplot, the snippet image is generated with the outlines of the annuli around the sources.

7. For convenience, each source is numbered according to their corresponding source ID in the sources table. This is to help the user visually identify the corresponding rows of unwanted sources.

In the case where the user wants to make table revisions but prefers not to produce a visual, a second optional function was created in pair with the View function. Called Revise, this mirrors the mechanics of the View function. It takes an externally edited source table passed as a parameter and updates the relevant internal variables for later use. It is essentially identical to the View function, but skips the plotting steps.

Finally, the concluding custom function in the photometry class is Magnitudes:

1. The areas of overlap between the inner radial circle and outer radial circle of an annulus are calculated using the radii defined in the Sources function.

2. Within each annulus, the background statistics are calculated with sigma clipping to exclude extreme outliers in messy data.

3. The background is then subtracted from the total pixel value count within the annulus areas in order to derive background-subtracted source fluxes. These are then recorded in a new column of the photometry table and formatted for consistent output.

4. Iterating through the list of source IDs specified in the parameters, the sources are located in the source table.

5. The matching ID is then found in the photometry table to gather the corresponding magnitudes and append them to a list.

6. Finally, the list of requested magnitudes are returned along with the entire photometry table.

To accelerate access to specified sources and avoid redundancy, Magnitudes allows the user to execute this step in a single line of code. Using the established internal variables, it subtracts the background within the annuli and returns the requested magnitudes along with the entire photometry table.

3. DATA/EXPERIMENT/OBSERVATIONS

To observe the impacts of interacting galaxies on their star formation rates, NGC 4567 was selected as the interacting galaxy to observe, while M 58 was selected as the non-interacting galaxy. These objects were compared against each other by subtracting photometric data in the H-α band from the R-band. What's remaining is an indicator of the star formation rate activity.

Table 1. Summary Information of the Observed Objects

| Object	RA	Dec	Redshift (z)	Angular Size (arcmin)	Filters
NGC 4567	12:36:32.698	11:15:28.716	0.007523	2.88 2.24 88	R, G, I, H-α
NGC 4568	12:36:32.698	11:15:28.716	0.00744	4.57 2.40	R, G, I, H-α
M 58	12:37:43.5	11:49:06	0.005066	5.62 4.37 88	R, G, H-α

Data for this project was gathered in two observation runs within three days of each other. With remote control of the ARCSAT telescope at APO, several accounts of photometric images of NGC 4567 and M 58 were taken in the G, H-α, R, and I bands on a Charge-Coupled Device (CCD). Along with the calibration frames (biases, flats, darks) taken, each file was exported as a .fits file and visually inspected with SAODS9 during the observing session. The weather was clear on both nights and the sky had low moon illumination. The second night of observation was windy at the end of the shift.

During the first observation shift, the group experimented with various exposure times to determine the ideal flux values at the center of NGC 4567. To check, the obtained fits files were opened in SAODS9 and inspected manually during the observing session. Starting with an exposure time of 60 seconds and 90 seconds, it was determined through manual inspection that higher exposure times would be optimal for the use of the images. The majority of the photos were taken with an exposure time of 600s, and some were taken at 900s.

Following the observing sessions, a preliminary step of viewing the raw images was done to explore the mechanics of FITS files and to gain a visual understanding of how the image looks before data reduction. During this step, a custom function was used (not previously mentioned) to iterate through files and view each frame before stacking. During this inspection, the importance of using a package that can account for physical coordinates became more apparent. Between raw images for each filter, a slight shift became noticeable. It is unknown whether the shift came from the telescope itself or by other means. With the use of the CCDProc package in the custom image stacking function, this shift was accounted for during combination by converting pixel values to the World Coordinate System (WCS).

$$Calibrated = \frac{RawStack - MasterBias - MasterDark}{NormalizedMasterFlat} \tag{1}$$

To pre-process the data, the raw images and flats were stacked into their respective filters, and masters were created for the biases and darks. The flat frames were each normalized with itself before creating a master stack. To conclude the data pre-processing, reductions were done using the array return feature of the custom stacking formula. Once each of the dark, bias, and flat frames were saved in array variables, the stacks of image data were calibrated by following the above formula (1) and writing the calibrated data for each filter to a new FITS file.
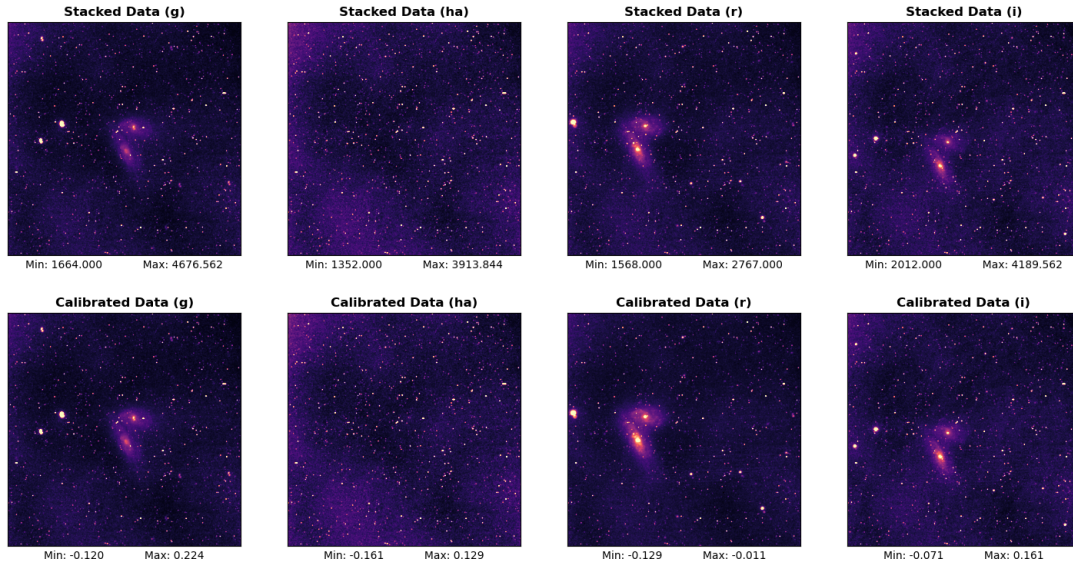
Figure 1. Comparison of raw stacked images and calibrated images for NGC 4567, plotted in Python with Z-scaling, Linear stretching, and the magma colormap between the 1st and 99.75th percentiles. Magnitude values are provided on the bottom. A render of the full size image is shown to allow for full context of resolution, object drifting, and the image data used in this project.

Once calibrated and saved, the de-noised images were viewed for a final quality inspection. It was observed that between the raw stacked images and the calibrated images, there was not a significant visual difference between them. However, the magnitudes in the raw and calibrated images greatly varied, with the raw images at values in the thousands, while the calibrated images had pixel values quantified in small, fractional values. To generate a plot of the full images, it was determined that a Z-scaling application with linear stretching was the most optimal, as shown in Figure 1. The same settings were applied to M 58's images, resulting in similar quality and pixel values. The drift of the objects across the image is also more noticeable with this side-by-side comparison of the Butterfly Galaxies across various filters and exposure times. To gain a further understanding of the pixel value distributions, the histogram in Figure 2 already begins to show the differences between the objects of NGC 4567 & NGC 4568 and M 58.
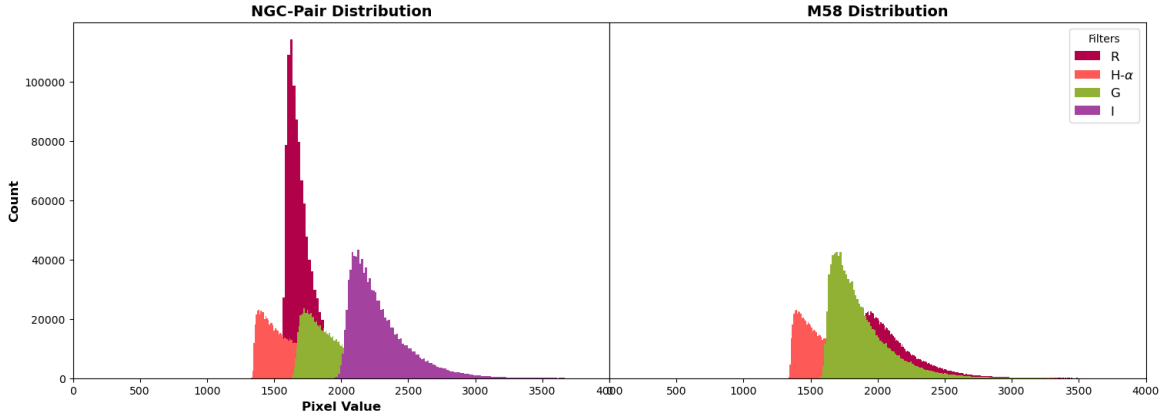
Figure 2. Histogram showing the color value distributions of the Butterfly Galaxies calibrated image stack and the M 58 calibrated image stack.

It is interesting to note the extreme differences in the R-band pixel counts, though perhaps not as surprising, considering the light received from M 58 is of a single galaxy as opposed to a pair of interacting galaxies. However, another curious observation is the striking parallelity of pixel values for H-α in both NGC 4567 & NGC 4568 and M 58 galaxies. Of course, this solidified the eagerness in investigating the comparison of stellar formation rates between the Butterfly Galaxies and M 58. From this initial visualization, the star formation rates between the Butterfly Galaxies seems disproportional considering the presence of two galaxies, though this could also be affected due to their interacting nature.

The star formation rates of NGC 4567 and M 58 were then obtained by subtracting the H-α image data from the R-band image data, and re-plotted with a view of their maximum flux values, shown later in Figure 4. The difference of the image data between the R and H-α filters are used to compare and observe the impacts of interacting galaxies and star formation rates. With the use of histograms, a numerical analysis could then be done to compare the stellar formation rates of a pair of interacting galaxies and a non-interacting galaxy.

4. RESULTS AND DISCUSSION

As seen in Figure 2, it was an interesting note to see the pixel counts for both objects in each filter. However, additional context about the two objects is important for further analysis in understanding the relationship between interacting galaxies and stellar formation rates.

It is somewhat surprising to see a hint of stellar formation in both objects despite its anticipation among the interacting galaxies. They are both noted (1) to have lower redshifts (z¡1), where it has been observed that peak activity occurs at the epoch transitioning from z=1 to z=2 (Madau et al. (1996)). However, it is also important to note that NGC 4567 and NGC 4568 are connected by a tidal interaction.

For the Butterfly Galaxies, their gravitational pull on each other causes their gases to collide with each other. Although they are separated by 6 kpc, this young interacting pair has comparable velocities and are close enough to create higher densities of interstellar medium (ISM). A peculiar characteristic of NGC 4568 (bottom) is its spiral tail extending from the southern region towards NGC 4567 (top). It is also noted that the molecular gas within this southern region extends further than the arms in the northern distribution. This characteristic supports the idea that there is enough gravitational ISM compression between the galaxies, increasing the density of molecular gases and thus triggering stellar formation activity (Nehlig, F. et al. (2016)).

The core of M 58, though relatively dim for a spiral galaxy, has high stellar formation activity. Its high activity categorizes M 58 as a Seyfert type 2 classification, complete with a supermassive black hole at the center. The stellar formation in this galaxy is driven by Active Galactic Nuclei (AGN) feedback which impacts the molecular gas in star forming regions (Lopez et al. (2022)). A quite violent energy release, the study of AGN feedback from supermassive black holes expands its own area of research. Despite its surrounding environmental challenges, the stellar formation rate of M 58 strongly withstands them and continues at high activity.
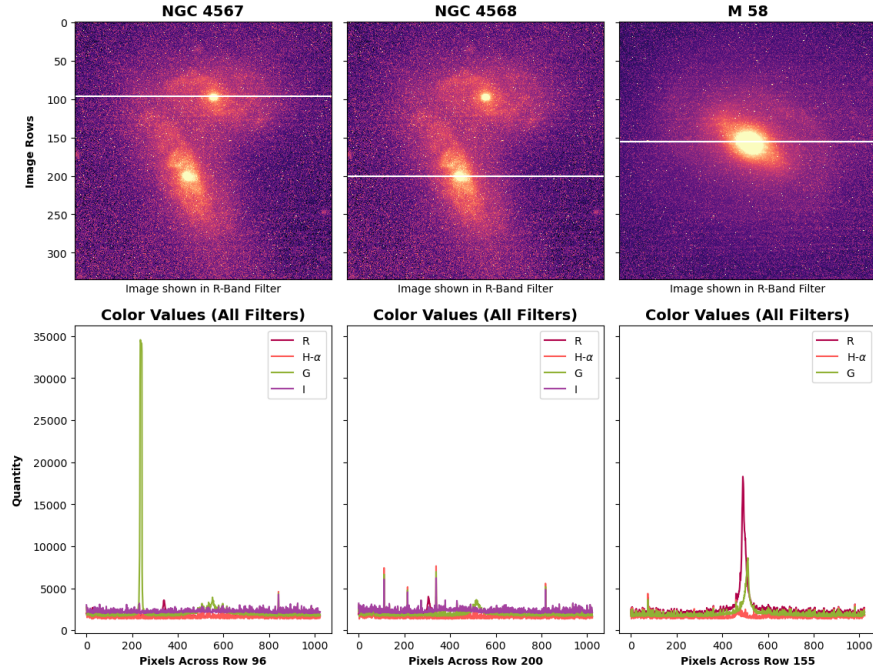
Figure 3. Comparison of color values in each filter of objects NGC 4567, NGC 4568, and M 58. Plot depicts the values selected from a row that bisects the galactic center.

To look for hints of stellar formation rate activity, the row of pixels that intersects the galactic centers of each object was selected to analyze the color values across all filters (Figure 3). The line segment indicates the row array of pixels extracted from the image data - and, as shown, the color values between the Butterfly Galaxies and M 58 look quite different in quantity and shape.

Considering that M 58 is a spiral galaxy with a supermassive black hole at the core, it is no surprise that there is a strong spike across all filters at the center of the galaxy. On the contrary, it was surprising to see such a high quantity of green color values for NGC 4567 - however, this may be due to data pollution and influence from its partner, NGC 4568. This quantifiable comparison also demonstrates the striking similarities in H-α color values between the pair and the lone galaxy. Indicated by the salmon color, it is difficult to identify stark differences in the shape of the curves, which leads to the idea of considering their similarities in stellar formation rate activity. To explore further, the stellar formation rates were plotted over a histogram in Figure 4:
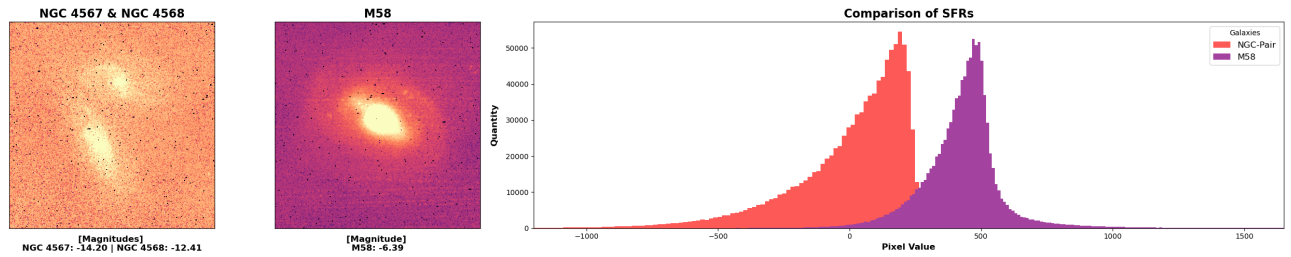
Figure 4. A histogram of pixel quantities of the derived stellar formation rates between the Butterfly Galaxies and M 58

Additionally, the magnitudes of the three observed objects were calculated as follows:

1. NGC 4567: -14.20

2. NGC 4568: -12.41

3. M58: -6.39

It is evident that between the Butterfly Galaxies and M 58, there is the potential for strikingly similar stellar formation rate activity. As members of the Virgo Cluster, they may experience similar environmental effects due to the nature of it being a large cluster. Among them, a high number of spiral galaxies represents the majority following the high population of dwarf elliptical galaxies. Their structures differ in nature, however, as the Butterfly Galaxies are growing in activity as they continue to interact, while the activity of M 58 continues to be challenged by environmental features as well as its own. M 58 is impacted by interstellar medium that strips away its free hydrogen, removing the fuel needed to form new stars. Its bar structure also causes gas to gather at the center nucleus, causing a potential for a burst of activity (Binggeli (????)).

5. CONCLUSION

In an attempt to study the stellar formation rates of interacting galaxies, the Butterfly Galaxies (NGC 4567 and NGC 4568) were observed and compared to the Ring Bearer Galaxy M 58. To study the activity of these spiral galaxies, CCD images were taken in the R, G, I, and H-α filters, where the stellar formation rate was derived by subtracting the H-α values from the R-band. Although the characteristics between the two objects were generally different, it was observed that their stellar formation rates were similar. However, this is not to make a generalization of all interacting galaxies and their formation rates. To build upon this project, a further study of a collection of various objects should be analyzed and compared against each other to make a general characterization of stellar formation rates and their relationship with interacting galaxies.

REFERENCES

Astropy Collaboration, Price-Whelan, A. M., Lim, P. L., et al. 2022, The Astrophysical Journal, 935

Binggeli, B. ????, NASA/IPAC Extragalactic Database. https://ned.ipac.caltech.edu/level5/ESSAYS/Binggeli/binggeli.html#Table%201

Boquien, M., Buat, V., & Perret, V. 2014, Astronomy amp; Astrophysics, 571, A72, doi: 10.1051/0004-6361/201424441

Glazebrook, K., Blake, C., Economou, F., Lilly, S., & Colless, M. 1999, Monthly Notices of the Royal Astronomical Society, 306, 843, doi: 10.1046/j.1365-8711.1999.02576.x

Hartmut Frommert, C. K. 1996, Students for the Exploration and Development of Space (SEDS). http://www.messier.seds.org/m/m058.html

Herschel, W. 1786. http://doi.org/10.1098/rstl.1786.0027

James, P. A., Shane, N. S., Beckman, J. E., et al. 2004, Astronomy amp; Astrophysics, 414, 23–43, doi: 10.1051/0004-6361:20031568

Lopez, I. E., Ogle, P., & Reynaldi, V. 2022, Resolving the extended emission of H2 on M58, Zenodo, doi: 10.5281/zenodo.6421835

Madau, P., Ferguson, H. C., Dickinson, M. E., et al. 1996, Monthly Notices of the Royal Astronomical Society, 283, 1388, doi: 10.1093/mnras/283.4.1388

Nehlig, F., Vollmer, B., & Braine, J. 2016, AA, 587, A108, doi: 10.1051/0004-6361/201527021

Tacchella, S., Smith, A., Kannan, R., et al. 2022, Monthly Notices of the Royal Astronomical Society, 513, 2904, doi: 10.1093/mnras/stac818